The Kondo Effect in the Presence of Ferromagnetism

Abhay N. Pasupathy *et al.*

Science **306**, 86 (2004);
DOI: 10.1126/science.1102068

41. M. Yanovsky, S. Kay, *Nature Rev. Mol. Cell Biol.* **4**, 265 (2003).
42. C. Leblanc, A. Falciatore, C. Bowler, *Plant Mol. Biol.* **40**, 1031 (1999).
43. M. Ragni, M. Ribera, *J. Plankton Res.* **26**, 433 (2004).
44. X.-P. Li *et al.*, *Nature* **403**, 391 (2000).
45. B. Palenik *et al.*, *Nature* **424**, 1037 (2003).
46. J. K. Moore, S. C. Doney, D. M. Glover, I. Y. Fung, *Deep-Sea Res. II* **49**, 463 (2002).
47. P. W. Boyd *et al.*, *Nature* **407**, 695 (2000).
48. K. H. Coale *et al.*, *Science* **304**, 408 (2004).
49. N. J. Robinson, C. M. Procter, E. L. Connolly, M. L. Guerinot, *Nature* **397**, 694 (1999).
50. This work was performed under the auspices of the U.S. Department of Energy's (DOE) Office of Science, Biological, and Environmental Research Program and by the University of California, Lawrence Livermore National Laboratory under Contract No. W-7405-Eng-48, Lawrence Berkeley National Laboratory under contract No. DE-AC03-76SF00098, and Los Alamos National Laboratory under contract No. W-7405-ENG-36.; and DOE (DE-FG03-02ER63471 to E.V.A.), European Union Margens (QLRT-2001-01226 to C.B.), the CNRS Atip program (2JE144 to C.B.), and the U.S. Environmental Protection Agency (R827107-01-0, Basic to B.P., M.H.).

Supporting Online Material
www.sciencemag.org/cgi/content/full/306/5693/79/DC1
Materials and Methods
Figs. S1 to S7
Tables S1 to S4
References

7 June 2004; accepted 17 August 2004

REPORTS

The Kondo Effect in the Presence of Ferromagnetism

Abhay N. Pasupathy,[1] Radoslaw C. Bialczak,[1] Jan Martinek,[2] Jacob E. Grose,[1] Luke A. K. Donev,[1] Paul L. McEuen,[1] Daniel C. Ralph[1]*

We measured Kondo-assisted tunneling via C_{60} molecules in contact with ferromagnetic nickel electrodes. Kondo correlations persisted despite the presence of ferromagnetism, but the Kondo peak in the differential conductance was split by an amount that decreased (even to zero) as the moments in the two electrodes were turned from parallel to antiparallel alignment. The splitting is too large to be explained by a local magnetic field. However, the voltage, temperature, and magnetic field dependence of the signals agree with predictions for an exchange splitting of the Kondo resonance. The Kondo effect leads to negative values of magnetoresistance, with magnitudes much larger than the Julliere estimate.

Measurements on individual quantum dots have in recent years provided a detailed understanding of the Kondo effect (*1–7*): the coupling between a localized spin and conduction electrons that serves as a fundamental model for understanding correlated-electron physics (*8*). Itinerant-electron ferromagnetism is an alternative correlated-electron state that can arise from Coulomb interactions between electrons. These two states ordinarily compete with each other; in heavy fermion systems, a phase transition is thought to exist between the Kondo and magnetic ground states (*9*). Calculations for the consequences of coupling between a Kondo-regime quantum dot and ferromagnetic electrodes have produced conflicting predictions (*10–14*). Experimentally, Kondo physics has not previously been studied in quantum dots with magnetic electrodes, despite work with both normal-metal (*1–6*) and superconducting (*7*) systems, because of difficulty in achieving sufficiently strong coupling between the dot and magnetic materials. We demonstrate here that C_{60} molecules can be strongly coupled to nickel (Ni) electrodes so as to exhibit the Kondo effect. Ferromagnetism can suppress Kondo-assisted tunneling, but Kondo correlations are still present within the ferromagnetic electrodes, and in particular situations the strong-coupling limit of the Kondo effect can still be achieved.

First, we compare measurements made using (magnetic) Ni and (nonmagnetic) gold (Au) electrodes, building on studies of single-electron transistors made using C_{60} (*15*) and previous measurements of Kondo-assisted tunneling using C_{60} in contact with Au electrodes (*6*). Our devices are made by using electron-beam lithography and liftoff to create electrodes that are 30 nm high and 50 nm wide at their narrowest point. After cleaning the electrodes in an oxygen plasma (0.25 W/cm^2 for 2 min), we deposit 50 μl of a dilute solution (≈100 μM) of C_{60} in toluene over a 30-mm^2 area of the chip and allow the solvent to evaporate. We cool the chip to 1.5 K and then use an electromigration procedure (*16*) to create a nanometer-scale break in the wire. One or more molecules of C_{60} can bridge this gap. For C_{60} with nonmagnetic Au electrodes, some samples show featureless tunnel conduction or conventional high-resistance Coulomb blockade characteristics (*15*), but in approximately 20% of 100 junctions the differential conductance [$G(V) \equiv dI/dV \equiv 1/R(V)$] curves display a peak at $V = 0$ (Fig. 1A) (*6*) (V, voltage; I, current; R, resistance). This peak can be split by applying a magnetic field B, with an average g factor ≈ 2. These features are signatures of the Kondo effect in a spin-1/2 quantum dot (*1–6*). The Kondo signals were absent in a set of 40 control samples that underwent the same fabrication procedure, but without the C_{60} deposition.

For magnetic Ni electrodes, the shapes of the two electrodes were designed to give them different magnetic anisotropies, so that they undergo magnetic reversal at different values of B(*17*). We have experimented with several combinations of shapes and have had good success with the pattern shown in Fig. 1B. The magnetic properties of test electrodes were checked in the absence of any molecules, by measuring the magnetoresistance of tunnel junctions created by electromigration (Fig. 1C). The curves display hysteretic switching features familiar from previous studies of magnetic tunnel junctions (*18*), demonstrating that we can control the relative orientation of the magnetic moments in the two electrodes between parallel (P) and approximately antiparallel (AP) alignment. We can compare the magnitude of the junction magnetoresistance (JMR) to the Julliere estimate (*19*): JMR $\equiv (R_{AP} - R_P)/R_P = 2P^2/(1 - P^2)$, where R_P is the resistance when the magnetizations are parallel, R_{AP} is the resistance when the magnetizations are antiparallel, and P is the tunneling spin polarization. Using $P = 0.31$ measured for thin films of Ni with aluminum oxide tunnel

[1]Laboratory of Atomic and Solid State Physics, Cornell University, Ithaca, NY 14853, USA. [2]Institut für Theoretische Festkörperphysik, Universität Karlsruhe, 76128 Karlsruhe, Germany; Institute for Materials Research, Tohoku University, Sendai 980–8577, Japan; and Institute of Molecular Physics, Polish Academy of Sciences, 60–179 Poznań, Poland.

*To whom correspondence should be addressed. E-mail: ralph@ccmr.cornell.edu

barriers (*20*), the Julliere estimate is JMR = 21%. The sample shown in Fig. 1C has JMR = 19%, and for other samples we find values in the range from 10 to 19%.

After we performed electromigration on Ni samples with C_{60} adsorbed on them, about 5% of the devices exhibited simple high-resistance Coulomb blockade characteristics (*15*); and in approximately 3% of 1200 total devices, we observed $G(V)$ versus V curves similar to those in Fig. 2, A and C. Instead of having a single peak in $G(V)$ centered at $V = 0$ as observed for Kondo tunneling with Au electrodes, when the moments of the Ni electrodes were aligned parallel by a small applied field, we observed two peaks in $G(V)$, approximately symmetric about $V = 0$ and with similar amplitudes and widths, situated atop a background that can be asymmetric in V. These characteristics are different from Coulomb blockade conductance peaks (*21*).

The split peaks in Figure 2 display a strong dependence on the relative orientation of the magnetic moments in the two electrodes. Figure 2B shows a color scale plot of $G(V,B)$ for sample 1 as a function of B (y axis) and V (x axis), recorded at 1.5 K. B is swept from negative to positive values. When $B < -10$ mT, there are two peaks in $G(V)$ with a splitting $\Delta V_P = 16$ mV that displays only a weak dependence on B. At $B = -10$ mT, there is an abrupt switch, at which point the splitting is reduced to $\Delta V_{AP} = 7.6$ mV. In the range -10 mT $< B < 200$ mT, the splitting between the peaks gradually increases. At $B = 200$ mT, there is a second abrupt switching event, and the $G(V)$ curves for larger positive fields are the same as at large negative fields. When the sweep direction for B is reversed, the $G(V,B)$ plots exhibit magnetic hysteresis, with the switching fields reversed about $B = 0$. We can therefore associate these changes with the relative orientation of the moments in the two magnetic electrodes. For negative B in Fig. 2B, the moments are parallel and the peak splitting is large. At $B = -10$ mT, one moment reverses to give an approximately antiparallel configuration with a smaller splitting. On further increasing B, the other moment rotates gradually, and then at $B = 200$ mT the second moment reverses to restore the P configuration.

Figure 2, C and D, shows a similar progression as a function of B for sample 2. Again there is a large splitting, $\Delta V_P = 18$ mV, for parallel moments in the electrodes, but in the AP configuration the splitting is reduced sufficiently that only one peak in $G(V)$ is resolvable. The lack of splitting for the AP case indicates that the strong-coupling Kondo effect is possible even in the presence of ferromagnetic electrodes.

The splittings between the conductance peaks are too large to be associated with Zeeman splitting of the Kondo resonance in a local magnetic field. Assuming a g factor of 2, a splitting $\Delta V_P = 16$ mV corresponds to a magnetic field of 70 T. An upper limit on the local magnetic field that can be generated by the magnetic electrodes in the small gap is given by their magnetization, 0.6 T for Ni.

The magnetic field dependence of our split peaks is in excellent agreement with some recent predictions that the interaction of a quantum dot with spin-polarized electrodes can produce a splitting of the Kondo resonance (*12–14*). In this model, the conductance of a single-level quantum dot is determined by the tunneling spin polarizations P_L, P_R and the couplings Γ_L, Γ_R between the dot and the left and right electrodes. We will assume that polarizations are $P_L = P_R = P = 0.31$ (as for a Ni junction) for the P orientation and $P_L = -P_R = P$ for the AP orientation. Because of quantum charge fluctuations, the

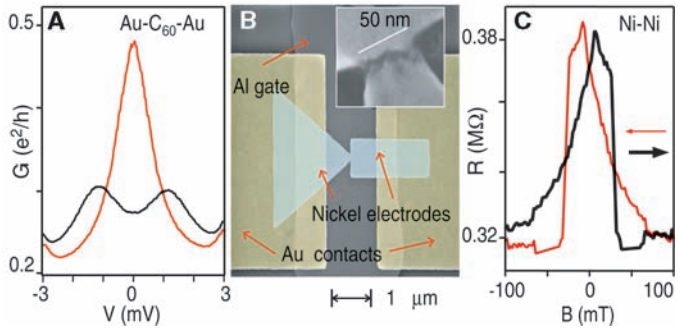

Fig. 1. (**A**) Kondo signal for C_{60} with Au electrodes at $T = 1.5$ K. At $B = 0$ (red line), there is a zero-bias peak in $G(V)$ that becomes split for $B = 10$ T (black line). (**B**) Scanning electron micrograph of a Ni break junction. The magnetic field is applied in the horizontal direction. (**Inset**) Close-up of the junction region after electromigration. (**C**) Tunneling magnetoresistance near $V = 0$ at $T = 4.2$ K of a Ni contact after electromigration, with no C_{60} molecule present.

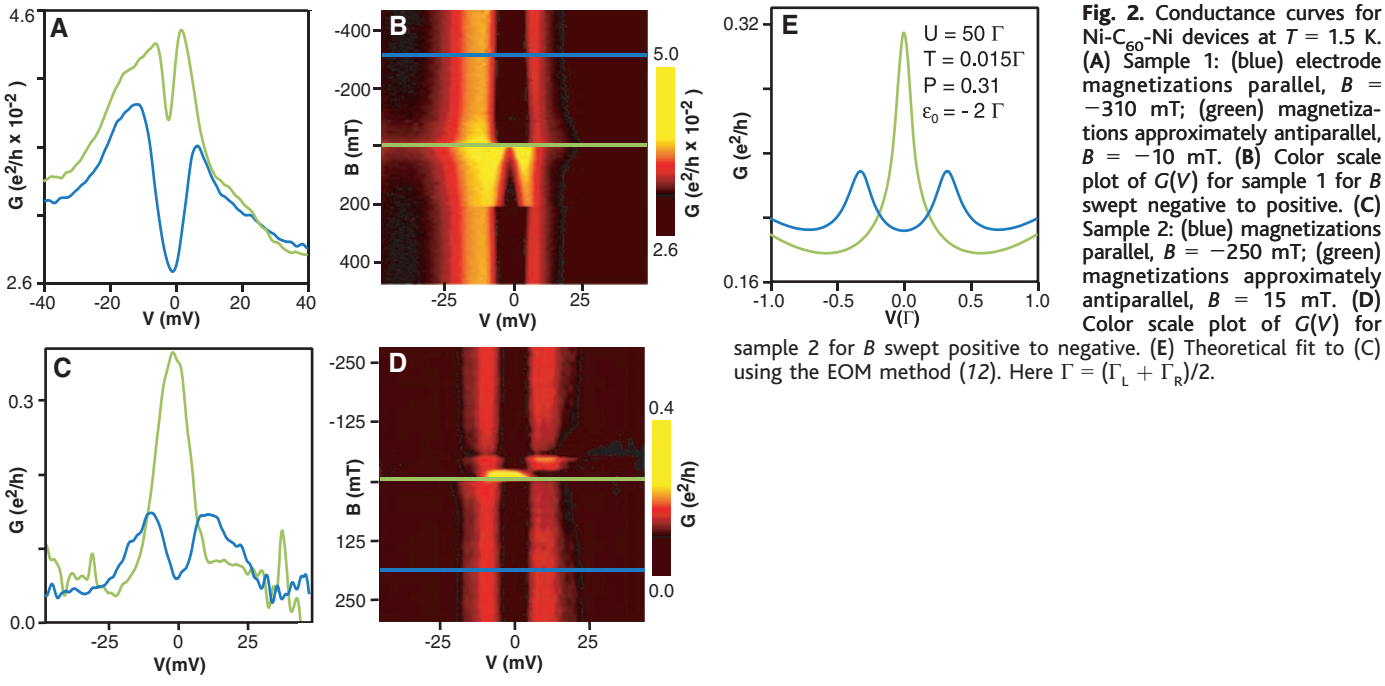

Fig. 2. Conductance curves for Ni-C_{60}-Ni devices at $T = 1.5$ K. (**A**) Sample 1: (blue) electrode magnetizations parallel, $B = -310$ mT; (green) magnetizations approximately antiparallel, $B = -10$ mT. (**B**) Color scale plot of $G(V)$ for sample 1 for B swept negative to positive. (**C**) Sample 2: (blue) magnetizations parallel, $B = -250$ mT; (green) magnetizations approximately antiparallel, $B = 15$ mT. (**D**) Color scale plot of $G(V)$ for sample 2 for B swept positive to negative. (**E**) Theoretical fit to (C) using the EOM method (*12*). Here $\Gamma = (\Gamma_L + \Gamma_R)/2$.

spin asymmetry in the coupling to the electrodes produces a spin-dependent renormalization of the dot's levels ε_σ (bare value ε_0), breaking the spin degeneracy: $\varepsilon_\uparrow \neq \varepsilon_\downarrow$. This results in a splitting of the $G(V)$ curve which (in the general case when an external field B is applied) has the value (*13*)

$$e\Delta V = 2\,|\,g\mu_B B + a\sum_{r=L,R} P_r\Gamma_r\,| \qquad (1)$$

Here μ_B is the Bohr magneton and a is a constant of order unity whose magnitude and sign depend on the charging energy U, ε_0, and the detailed band structure (*22*). If the magnetizations are AP and the dot has equal couplings to both electrodes $\Gamma_L = \Gamma_R$, the exchange interactions from the two electrodes are compensated. In this situation, the strong-coupling Kondo effect is restored despite the spin polarization in the leads, and the splitting is predicted to be reduced to zero near $B = 0$ (Fig. 2E). However, when one takes into account that typically $\Gamma_L \neq \Gamma_R$, then the low-B peak splittings in the P and AP orientations should be (assuming $\Gamma_L > \Gamma_R$)

$$e\Delta V_P = 2aP(\Gamma_L + \Gamma_R) \qquad (2)$$

$$e\Delta V_{AP} = 2aP(\Gamma_L - \Gamma_R) \qquad (3)$$

These results are consistent with our measurements of larger splittings for parallel moments and smaller but generally nonzero splittings in the AP case (*23*).

For sample 1, Fig. 2B and Eqs. 2 and 3 together provide an estimate for the tunnel coupling ratio $\Gamma_L/\Gamma_R = (\Delta V_P + \Delta V_{AP})/(\Delta V_P - \Delta V_{AP}) \approx 3$. If we pick a typical value of $aP \approx 0.15$ (*12–14*) we can estimate $\Gamma_L \approx 45$ meV and $\Gamma_R \approx 15$ meV. For sample 2, for which no splitting was resolved in the AP state, we can set the limit $\Gamma_L/\Gamma_R < 2$, with $\Gamma_L, \Gamma_R \approx 30$ meV. These numbers will change according to the value of aP assumed, according to Eq. 1. To obtain other estimates of device parameters, we have performed theoretical fits of $G(V)$ using the equations-of-motion (EOM) technique (*12*). A plot for sample 2 in the parallel (solid) and antiparallel (dashed) magnetization orientations is shown in Fig. 2E. The parameters used are $\Gamma = 30$ meV, $\varepsilon_0 = -60$ meV, and $U = 1.5$ eV. The fits are relatively insensitive to changes in U by up to an order of magnitude. Γ and ε_0 are determined to about a factor of 2 once P_L, P_R are set. Values of the same order of magnitude are extracted for sample 1.

Further confirmation that the split peaks in $G(V)$ are associated with Kondo physics comes from their dependence on temperature (T) and B. In order to measure changes at cryogenic temperatures and laboratory magnetic fields, one must focus on samples with narrow-in-V conductance peaks, associated with small Kondo temperatures (T_K) (Fig. 3). Theory indicates that the T dependence of the peak conductance around T_K should be approximately logarithmic even when the Kondo resonance is split (*24*). This is what we observe, for both parallel (Fig. 3A, sample 3) and antiparallel (Fig. 3B, sample 4) alignment of the electrode moments.

In Fig. 3C, we show how an applied magnetic field affects the $G(V)$ versus V curves for sample 4, which has a particularly narrow peak width (0.3 meV). For all values of B displayed, the electrode moments are approximately parallel. The extracted peak positions are plotted in Fig. 3D. The peak spacing increases approximately linearly with $|B|$ with a g factor of 1.8 ± 0.3. Assuming that the tunneling polarization of Ni is positive (*20*), this would imply that the sign of a in Eq. 1 is positive (*22*). There is a residual zero-field splitting of $\Delta V_P = 0.14 \pm 0.06$ mV.

We have shown that coupling to the magnetic electrodes produces a large local exchange field on the quantum dot (greater than 50 T) that can be modulated by using a small external magnetic field (<100 mT) to control the relative orientation of the moments in the electrodes. We find that this amplification can dramatically enhance the JMR, in agreement with theoretical predictions (*12*). As a magnetic field is used to turn the electrode moments from parallel to antiparallel alignment, the zero-bias JMR is −38% for sample 1 (Fig. 4A) and −80% for sample 2 (Fig. 4B). The sign of the JMR is negative, opposite to the typical behavior in magnetic tunnel junctions, and the magnitude is much larger than the Julliere value of 21%. This happens because the Kondo resonance occurs closer to the Fermi energy for the antiparallel magnetization orientation, thus enhancing its conductance (*12*). A different mechanism for negative values of JMR has been discussed previously in connection with sequential electron tunneling via localized charge states (*25*), but the magnitude of this effect is smaller than the Kondo mechanism we report.

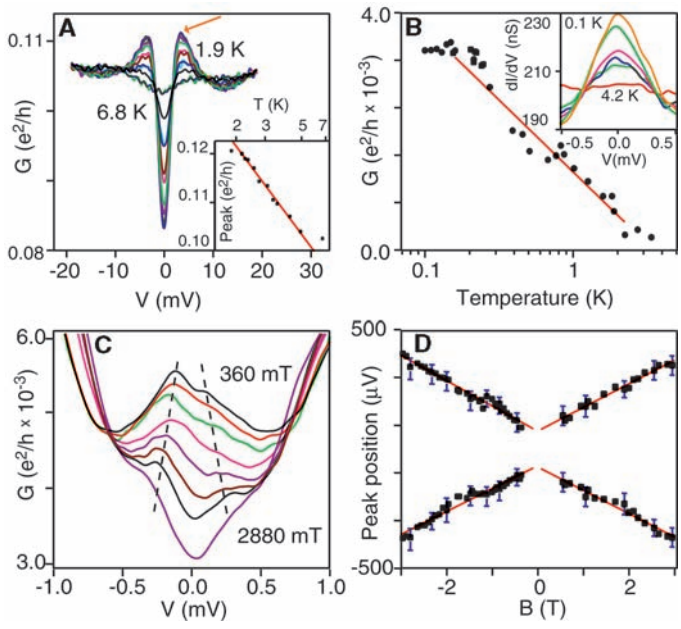

Fig. 3. (**A**) T dependence of $G(V)$ for Ni-C_{60}-Ni sample 3 with electrode moments parallel, B = 250 mT. (**Inset**) Peak conductance (red arrow) versus T for these curves. (**B**) Fitted height above background for Kondo peak versus T for Ni-C_{60}-Ni sample 4 with electrode moments approximately antiparallel, B = 10 mT. (**C**) $G(V)$ for sample 4 at 100 mK, at equally spaced values of B for which the electrode moments are parallel. (**D**) Peak positions extracted from (C). Typical error bars are shown.

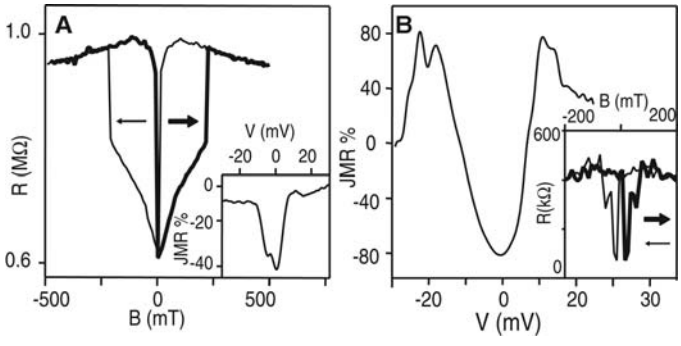

Fig. 4. $V = 0$ magnetoresistance at T = 1.5 K and the JMR as a function of V for two Ni-C_{60}-Ni samples. (**A**) Sample 1. (**B**) Sample 2.

References and Notes

1. D. Goldhaber-Gordon *et al.*, *Nature* **391**, 156 (1998).
2. S. M. Cronenwett, T. H. Oosterkamp, L. P. Kouwenhoven, *Science* **281**, 540 (1998).
3. J. Nygard, D. H. Cobden, P. E. Lindelof, *Nature* **408**, 342 (2000).
4. J. Park *et al.*, *Nature* **417**, 722 (2002).
5. W. Liang *et al.*, *Nature* **417**, 725 (2002).
6. L. H. Yu, D. Natelson, *Nano Lett.* **4**, 79 (2004).
7. M. R. Buitelaar, T. Nussbaumer, C. Schonenberger, *Phys. Rev. Lett.* **89**, 256801 (2002).
8. A. C. Hewson, *The Kondo Problem to Heavy Fermions* (Cambridge Univ. Press, Cambridge, 1993).

9. In the Kondo ground state, the localized spin is screened by the conduction electrons, suppressing magnetic interactions. In the magnetic ground state, spin degeneracy is broken, which suppresses spin fluctuations and Kondo correlations (*26*).
10. N. Sergueev *et al.*, *Phys. Rev. B* **65**, 165303 (2002).
11. P. Zhang, Q.-K. Xue, Y. Wang, X. C. Xie, *Phys. Rev. Lett.* **89**, 286803 (2002).
12. J. Martinek *et al.*, *Phys. Rev. Lett.* **91**, 127203 (2003).
13. J. Martinek *et al.*, *Phys. Rev. Lett.* **91**, 247202 (2003).
14. M.-S. Choi, D. Sanchez, R. Lopez, *Phys. Rev. Lett.* **92**, 056601 (2004).
15. H. Park *et al.*, *Nature* **407**, 57 (2000).
16. H. Park *et al.*, *Appl. Phys. Lett.* **75**, 301 (1999).
17. R. P. Cowburn, *J. Phys. D* **33**, R1 (2000).
18. E. Y. Tsymbal, O. N. Mryasov, P. R. LeClair, *J. Phys. Cond. Mat.* **15**, R109 (2003).
19. M. Julliere, *Phys. Lett. A* **54**, 225 (1955).
20. D. J. Monsma, S. S. P. Parkin, *Appl. Phys. Lett.* **77**, 720 (2000).
21. Coulomb blockade conductance peaks are not generally symmetric in V nor do they have similar heights for positive and negative bias, because the capacitances and resistances to the two electrodes are different in general (*27*).
22. J. Martinek *et al.*, http://arxiv.org/abs/cond-mat/0406323 (2004).
23. In addition to the Kondo signals, tunneling through the independent electron resonances should be expected to produce peaks in $G(V)$ centered at the Coulomb blockade energy thresholds, with widths on the order of Γ. However, we do not usually resolve these Coulomb blockade peaks in the Kondo samples. Estimates of Γ as large as many tens of milli–electron volts suggest that they would be difficult to observe. Nevertheless, we do expect that electron tunneling through these broad single-electron resonances contributes to the asymmetric conductance background underlying the Kondo signals.
24. J. Paaske, A. Rosch, P. Wölfle, *Phys. Rev. B* **69**, 155330 (2003).
25. E. Y. Tsymbal, A. Sokolov, I. F. Sabirianov, B. Doudin, *Phys. Rev. Lett.* **90**, 186602 (2003).
26. S. Doniach, *Phys. B* **91**, 231 (1977).
27. E. Bonet, M. M. Deshmukh, D. C. Ralph, *Phys. Rev. B* **65**, 045317 (2002).
28. We thank F. Kuemmeth for experimental help and J. Barnaś, L. Borda, P. Bruno, R. Bulla, J. von Delft, L. Glazman, H. Imamura, J. König, S. Maekawa, J. Petta, A. Rosch, G. Schön, M. Sindel, J. Stankowski, M. Vojta, and Y. Utsumi for discussions. This work was supported by NSF through the Cornell Center for Materials Research (grant DMR-0079992) and use of the Cornell NanoScale Facility; by the Defense Advanced Research Projects Agency/Office of Naval Research (grant N00173-03-1-G011); by the Army Research Office (grant DAAD19-01-1-0541); and by the Deutsche Forschungsgemeinshaft under the Center for Functional Nanostructures, "Spintronics" Research and Training Network of the European Community (EC) (grant RTN2-2001-00440), project PBZ/KBN/044/P03/2001 and EC contract G5MA-CT-2002-04049.

28 June 2004; accepted 11 August 2004

Extinct ^{244}Pu in Ancient Zircons

Grenville Turner,[1]* T. Mark Harrison,[2,3] Greg Holland,[1] Stephen J. Mojzsis,[4] Jamie Gilmour[1]

We have found evidence, in the form of fissiogenic xenon isotopes, for in situ decay of ^{244}Pu in individual 4.1- to 4.2-billion-year-old zircons from the Jack Hills region of Western Australia. Because of its short half-life, 82 million years, ^{244}Pu was extinct within 600 million years of Earth's formation. Detrital zircons are the only known relics to have survived from this period, and a study of their Pu geochemistry will allow us to date ancient metamorphic events and determine the terrestrial Pu/U ratio for comparison with the solar ratio.

The isotope ^{244}Pu is one of the longest lived of the so-called extinct isotopes that were present in the early solar system and that recorded nucleosynthetic processes immediately preceding its formation. This nuclide is produced solely in the r process, and its half-life is sufficiently long that it is expected to have been well-mixed locally within the galaxy in the sense that, on an 82-million-year (My) time scale, distances over which ^{244}Pu is dispersed are greater than the mean distance between supernovae in star-forming regions (*1*). On this basis, the equilibrium ratio of ^{244}Pu/^{238}U is expected to be equal to the ratio of the respective half-lives, i.e., 82/4450 = 0.018, multiplied by a number of order unity (related to the production rate of heavy precursors). A well-constrained initial value, combined with other key isotope abundance ratios (^{107}Pd, ^{129}I, ^{182}Hf, ^{235}U, ^{238}U, and ^{232}Th) would provide raw data with which to improve our understanding of the details of the r process and the timing of local nucleosynthetic events before the formation of the solar system (*1*–*5*).

Also, ^{244}Pu has a key role in understanding Earth evolution. Models of volatile transport within and from the mantle and of the origin and evolution of the atmosphere are influenced by inferences made from noble gas studies (*6*–*11*). A key parameter in these models is the Pu/U ratio, which determines the relative ingrowth of ^{136}Xe (from ^{244}Pu and ^{238}U fission) and ^{4}He (from U and Th decay) and hence quantifies the link between the Xe flux from the deep mantle source and that of He. Several attempts have been made to determine the overall ^{244}Pu/^{238}U ratio for the solar system (*12*, *13*) and to use ^{244}Pu as an early solar system chronometer (*14*–*16*); however, the solar value of ^{244}Pu/^{238}U is still uncertain within a factor of two, probably lying between 0.004 and 0.008. The discovery of terrestrial zircons with formation intervals between 4.0×10^9 and 4.4×10^9 years ago (Ga) offers an alternative way to resolve the issue. ^{238}U decay is the dominant source of fissiogenic xenon produced after 3.8 Ga, whereas ^{244}Pu decay dominates before 4.4 Ga. Between 4.0 and 4.4 Ga, contributions from ^{244}Pu and ^{238}U are expected to be comparable, and Pu/U can in principle be obtained directly from xenon analyses on samples with closure ages in this time interval. The ^{131}Xe/^{136}Xe ratio is particularly sensitive, varying between 0.085 for the spontaneous fission of ^{238}U and 0.246 for ^{244}Pu fission. A previous attempt to apply this method to large numbers of coeval zircons from

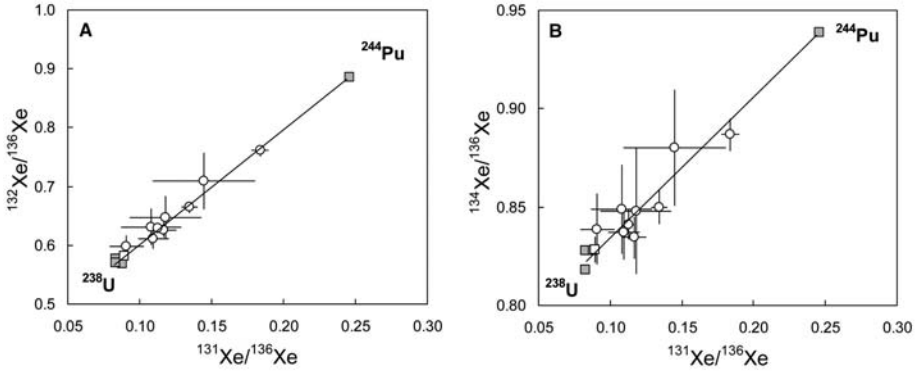

Fig. 1. After corrections for atmospheric Xe (fig. S4), the correlations of (**A**) ^{132}Xe/^{136}Xe with ^{131}Xe/^{136}Xe and of (**B**) ^{134}Xe/^{136}Xe with ^{131}Xe/^{136}Xe indicate that the remaining Xe is a two-component mixture produced by the spontaneous fission of ^{238}U and ^{244}Pu (solid squares). The highest ^{131}Xe/^{136}Xe ratio corresponds to a ^{244}Pu/^{238}U ratio of 0.0066 ± 0.0010 (calculated at 4560 Ma). Open circles are Jack Hills detrital zircons; open square is a 3.6-Gy-old zircon.

[1]Department of Earth Sciences, University of Manchester, Manchester M13 9PL, UK. [2]Research School of Earth Sciences, Australian National University, Canberra, ACT 0200, Australia. [3]Department of Earth and Space Sciences and Institute of Geophysics and Planetary Physics, University of California, Los Angeles, CA 90095, USA. [4]Department of Geological Sciences, Center for Astrobiology, University of Colorado, Boulder, CO 80309–0399, USA.

*To whom correspondence should be addressed. E-mail: grenville.turner@man.ac.uk